Catalysis Science & Technology

Accepted Manuscript

ROYAL SOCIETY OF CHEMISTRY

www.rsc.org/catalysis

QM/MM Study of The Mechanism of Reduction of 3-hydroxy-3-methylglutaryl co-enzyme A Catalyzed by Human HMG-CoA Reductase

*Eduardo F. Oliveira,[†] Nuno M.F.S.A. Cerqueira,[†] Maria J. Ramos,[†] Pedro A. Fernandes[†]**

[†]REQUIMTE, Departamento de Química e Bioquímica, Faculdade de Ciências, Universidade do Porto, s/n, Rua do Campo Alegre, 4169-007 Porto, Portugal.

**E-mail: pafernan@fc.up.pt*

Abstract

Detailing with atomistic resolution the reaction mechanism of human HMG-CoA reductase (HMG-CoA-R) might provide valuable insight for the development of new cholesterol-lowering drugs. On the pursue of that goal we developed three molecular models of human HMG-CoA-R with different active site protonation states and employed molecular dynamics (MD) and quantum mechanics/molecular mechanics (QM)/MM) calculations to detail the first reduction step, the rate-limiting step, of HMG-CoA-R. Our results predict an active site with a neutral glutamate (Glu559) as the most catalytic competent structure. The favored reaction pathway suggests the formation of a mevaldyl-CoA intermediate protonated by a conserved active site lysine (Lys691), corroborating previous site-directed mutagenesis studies. The conserved active site glutamate and aspartate residues (Glu559 and Asp767), along with the ribose moiety of NADPH, form a hydrogen bond network crucial to increase the stabilizing effect of Lys691 over the transition state.

Keywords: HMG-CoA Reductase; enzyme mechanism; enzymatic catalysis; Quantum Chemistry; Molecular Dynamics; QM/MM

Introduction

In this work we explore the first part of the elusive catalytic mechanism of 3-hydroxy-3-methylglutaryl-CoA reductase (HMG-CoA-R)(EC 1.1.1.34). HMG-CoA-R participates in the synthesis of isopentenyl pyrophosphate[1] which is then used as the precursor of cholesterol in addition to countless and structural diverse isoprenoids with multiple biochemical functions.[2] Due to its crucial role in cholesterol biosynthesis, HMG-CoA-R is the target of most anti-cholesterol drugs.

There are two evolutionarily divergent classes of HMG-CoA-Rs that can roughly be split into eukaryotes (class I) and prokaryotes (class II).[3] Those two classes conserve only ~14-20% sequence identity and present distinct structural features.[3,4] A conserved "cis-loop" motif (residues 682-694)[5] that forms part of the substrate binding pocket is present only in class I.[5,6] The differences in the active sites reverberate to differences in the stereochemistry of the reaction and in the affinity to bind statins, that range from the nanomolar in class I to the micromolar in class II.[7] These active site differences also suggest possible differences in the chemical mechanism and must be taken into account when analyzing the mechanistic studies.[4,8]

A better understanding of the HMG-CoA-R reaction mechanism will undoubtedly help the development of new drugs. However, HMG-CoA-R reaction mechanism is very complex, since it involves multiple chemical steps coupled with cofactor exchanges and large-scale domain motions of the multimeric enzyme. The generally accepted reaction sequence is depicted in Scheme 1. It is a two-step reduction of (S)-hydroxymethylglutaryl-CoA to (R)-mevalonate, at the expense of two molecules of NADPH and requires two proton donor residues.[9] The reaction free energy is close to zero, as the enzyme is seen to catalyze the reaction in the two directions.

In the last decades, a wealth of kinetic and isotope-labeling experiments, site-directed mutagenesis, crystal structures and, lately, computation modeling studies, have been used to propose increasingly complex reaction mechanisms.[10] Interpreting and interrelating these studies is sometimes difficult and requires careful attention, as they were done in both prokaryotic and eukaryotic enzymes and those enzymes present important differences.

To understand the protein role in the mechanism, Frimpong et al.[11] carried out an extensive mutagenesis study that has shown the importance of three active site residues (Glu559, Asp767, and His866, human HMG-CoA-R numbering). Each of these three mutants exhibited no more than 0.3% of the wild-type turnover, despite retaining similar K_m values for NADPH and (S)-HMG-CoA.[11] They suggested His866, with the help of Glu559, to protonate the CoA-S^- thiolate formed after the first hydride transfer. Asp767 was suggested to be the general acid that protonates iteratively the substrate thioester oxygen, facilitating both hydride transfers,[11] based on the essentially inactive performance of mutant Asp767Asn. A scheme of this proposal is shown in Supporting Information (Scheme S1).

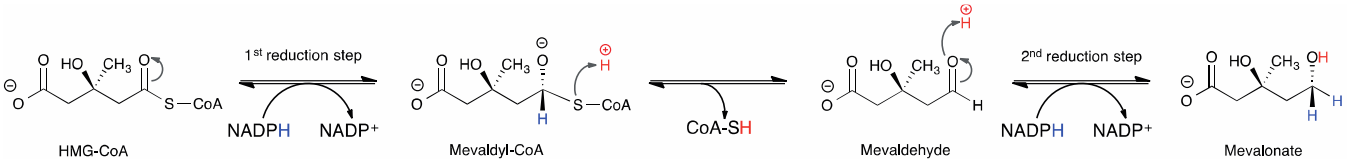

Scheme 1 - General reaction of HMG-CoA reductase. Protons colored in red come from acidic residues. H atoms in blue come from NADPH.

The first crystallographic structure of the human HMG-CoA-R was solved subsequently and revealed an active site geometry that was unfavorable for such mechanism,[5,6] as Glu559 side-chain (and not Asp767) is close to the thioester oxygen of HMG-CoA. The carboxylate of Asp767 is at 5.1 Å from the thioester oxygen and Lys691 amino group is located between Asp767 and the substrate, which renders improbable the role of the former as a proton donor.

Human enzyme mechanism proposal

Based on this structure, Istvan et al.[5] proposed a mechanism that started with a neutral Glu559 and a charged Asp767. They suggested Glu559 to be protonated as the two negative carboxylates are close enough (3.6-3.7 Å) for their pKas to be coupled, raising one and lowering the other. In their proposal, the negative charge in the thioester oxygen of HMG-CoA formed in the first reduction step is mainly stabilized by Lys691 with the help of

Glu559, through ionic hydrogen bonding and without protonation. Protonation of this oxygen (likely by Glu559) would only take place after mevaldehyde is formed (Scheme 2-A).[5]

The prokaryotic mechanism proposal

In another study, Tabernero et al.[8] obtained the class II HMG-CoA-R crystallographic structure of *pseudomonas mevalonii* (*P. mevalonii*). This structure corroborates the idea that Asp767 cannot protonate the carbonyl oxygen during the second reduction step, as Asp767 is too far apart and has Lys691* (Whenever possible we convert residues numbers to correspondent human numbering and mark them with an asterisk) in between, which hinders the direct protonation of the thioester oxygen, as proposed by Frimpong et al.[11] in the Syrian hamster enzyme.

Tabernero therefore supports that the lysine protonates mevaldehyde in the second reduction step and that it also forms a proton relay system with Glu559* and Asp767* to help the stabilization of the mevaldyl-CoA thioester (with or without protonation) after the first reduction step.[8] This lysine is highly conserved and site-directed mutagenesis experiments have shown severely attenuated reaction rates for the mutant[12,13] and led Bochar et al.[12] to suggest that an active site lysine should be a general acid during catalysis (Scheme 2-B).

Additionally, for the deacylation step, the proposal by Frimpong[11] that Glu559* protonates His866* is ruled out in the prokaryotic enzyme as Glu559* is more than 4 Å apart from His866*. Tabernero instead proposes that His866* is protonated by His385 (*P. mevalonii* numbering, as it has no equivalent in the human enzyme).

The prokaryotic mechanism modeled computationally

The importance of Lys691* and Glu559* for the reaction mechanism was also supported in a recent computational study using *P. mevalonii* enzyme as a model (Scheme 2-C).[14] This study reproduced the first and the second hydride transfer with a QM/MM ONIOM model starting from a neutral Glu559*. During the first hydride transfer, Glu559* fully transferred its proton to the thioester oxygen, forming mevaldyl-CoA. The same study considered that Glu559* should be again found neutral at the beginning of the second hydride transfer. In this step Glu559* protonates the mevaldyl-CoA to form mevalonate.

Therefore, during both hydride transfers, Glu559* and Lys691* form an oxyanion hole that stabilizes the developing negative charges in the transition states[14]. In both cases the carbonyl oxygen of the substrate is protonated upon hydride transfer (Scheme 2-C), and by the same residue (Glu559*). Considering that *P. mevalonii* HMG-CoA-R normally catalyzes the reverse reaction of human enzyme and the marked active site differences between class I and class II HMG-CoA-R,[3] it is far from obvious that there is a general mechanism for class I and class II HMG-CoA-R.

Beyond the questions regarding the identity of the residues implicated in the stabilization of the intermediates formed during the hydride transfers, materialized through the several reaction mechanism proposals found in the literature, there are also doubts regarding the identity of the intermediates formed along the reaction and the moment when the cofactor is exchanged. Several of the aforementioned proposals imply formation of mevaldyl-CoA, but neither free mevaldyl-CoA nor mevaldehyde are detected in solution during the overall cycle.[15] A structural analogue of the hemithioacetal, along with an oxidized co-factor, was found in a crystal structure from *P.*

mevalonii,[16] which supports the existence of a stable bound mevaldyl-CoA intermediate. Moreover, a previous study[14] indicated that a reaction pathway that produces a protonated hemithioacetal intermediate is slightly exothermic, while a deprotonated hemithioacetal, stabilized only through an oxyanion hole, is highly endothermic. The study concluded that two hydrogen bonds or a group acidic enough for proton transfer, were therefore required to stabilize the mevaldyl-CoA intermediate.

A systematic study of the several reaction mechanism possibilities on the human enzyme seems to be fundamental to shed light on this controversy. In this work we modeled three systems with different active site protonation states for the human HMG-CoA-R and tested several mechanistic alternatives for the first reduction of HMG-CoA. Two of these systems represent protonation states required to model the previous mechanistic proposals (Scheme 2). The additional system consists of a charged His752, which is absent in *P. mevalonii* structures. Along the study of the previous proposals we found conformations that suggested that a charged His752 might form an oxyanion hole with Lys691 to stabilize the negative charge developed in the thioester oxygen and decided to explore this mechanism. We then tested multiple potential reaction pathways in the three systems and the most viable are here presented. Besides the fundamental advance in understanding of the chemistry of HMG-CoA-R, this work also provides transition states (TS) structures that can be used as templates for high-throughput screening of new HMG-CoA-R inhibitors.[17]

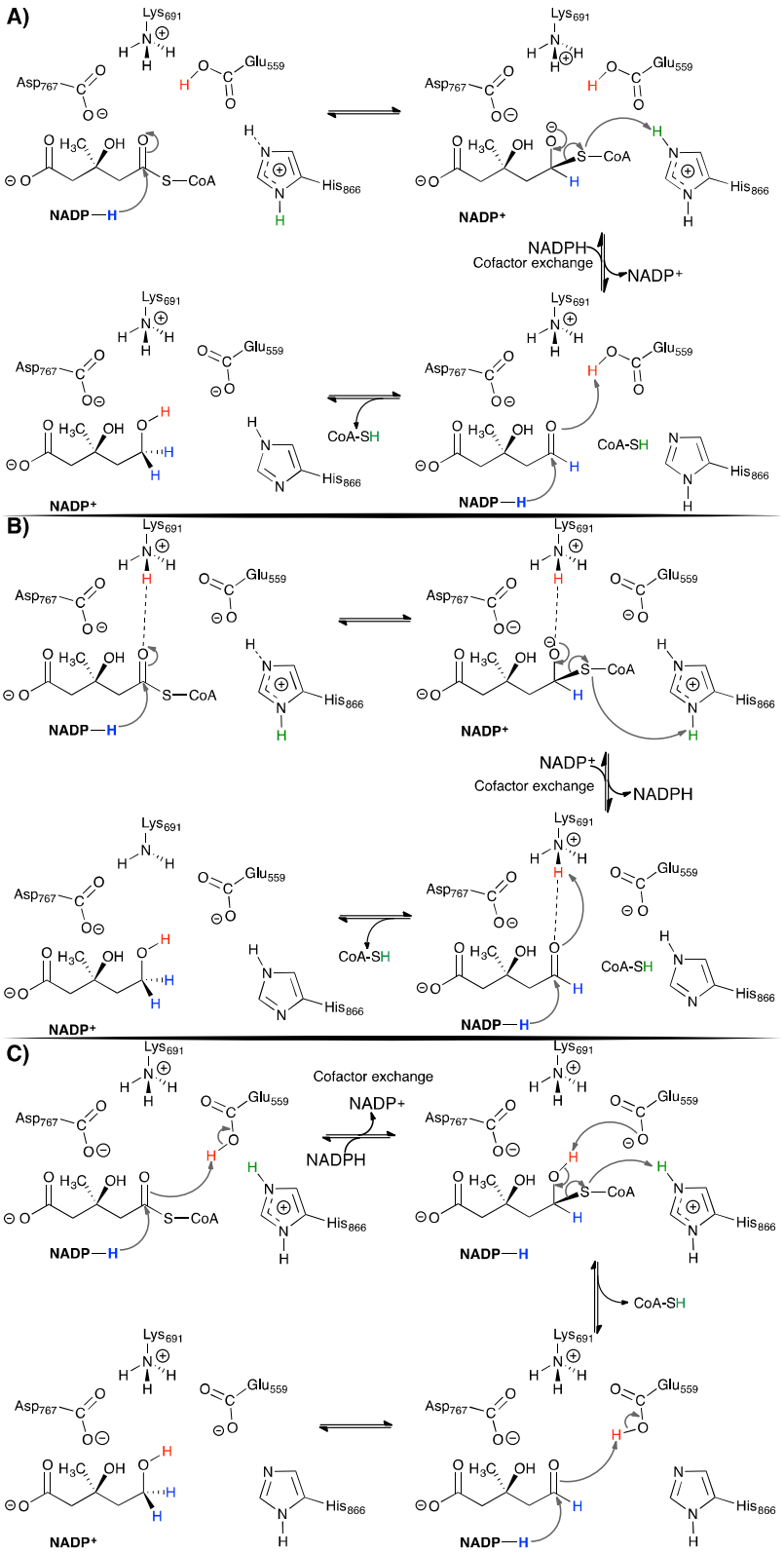

Scheme 2 - Different reaction mechanism of HMG-CoA-R as proposed by A) Istvan et al.[5] B) Tabernero et al.[8] C) Haines et al. This last was supported by theoretical calculations in the prokaryotic enzyme[14].

Theoretical Methods:

The overall line of work in this study can be summarized as follows:

1) Modeling of three HMG-CoA-R systems with different active site protonation states (**"Standard system"**, **"Glu559H system"** and **"His752H system"**);
2) Molecular dynamics (MD) simulation of the three systems to generate enzyme conformations adapted to the reactant state;
3) Comparison between the potential energy surfaces (PES) obtained with QM/MM calculations starting from the crystallographic conformation and from a conformation selected from the MD trajectory; This was made for every system.
4) Repeating the calculations of the PES of the reaction mechanism starting from fifteen enzyme conformations, for the system that was shown in 3) to have the most favorable kinetics.

1) Modeling the "Standard system", "Glu559H system" and "His752H system"

The catalytic portion of human HMG-CoA, after cleavage of the probable dimeric form found in the endoplasmatic reticulum,[18] is crystalized as a dimer of dimers. However, the dimer–dimer interface is distant from the active site and only the dimer of the molecule seems crucial for catalysis.[6,19] Taking this into account, we modeled the dimer form using chains C and D of the wild type structure with PDB id.: 1DQA (resolution of 2.0 Å). We selected the 1DQA structure for the following reasons: i) the binding of NADPH triggers a conformational change in the C-terminal helix that completes the closure of the active site and positions the His866 close to the sulfur atom of HMG-CoA, therefore this C-terminal helix is only ordered in structures containing the cofactor[6]; ii) the 1DQA structure is the unique human structure with bound NADP cofactor; iii) the active site we have selected, where CoA is bound to chain C and NADPH bound to chain D, has one of the longest C-terminal helix found in the 1DQA structure.

The other species found in the active site are a mevalonate analogue and CoA. We modeled the HMG-CoA substrate at the active site through superimposition with 1DQ9 structure (which has bound HMG-CoA) and transferred the substrate from one to the other.

The amino acid protonation states were first predicted with H++[20] and PROPKA[21] (pH=6.8) with divergent results, even for active site residues such as His866 or Glu559 (Table S1). The methods that provide pKas' inside enzymes are still not accurate enough to validate/exclude mechanisms by themselves, when applied to such large molecules, despite the efforts and progresses made by eminent people working in the field. The extremely anisotropic electrostatic environment, the limited number of well-known pKa's compared to the diversity of the environments, or the large number of titrable groups are some of the causes for the difficulty. Even though techniques such as thermodynamic integration could provide more reliable results for relative pKas,[22] their accuracy (and of the force fields) is still insufficient to result in solid conclusions about protonation states when subtle pKa differences are sought. Due to the lack of an accurate and reliable method for pKa prediction to resolve the controversy and since the differences in free energy between the different protonation states (for Glu559, His752 and Asp767)

are smaller than the differences between the chemical mechanisms they led to (see results), we opted to explore all possibilities and modeled explicitly three systems with different protonation states for Glu559, His752 and Asp767 residues, instead of choosing a particular one without very solid calculations. The chosen possibilities were those necessary to test the proposed mechanisms and reasonable within the enzyme environment. We assigned the most common protonation states at pH 6.8 for the remaining residues, except for the active site His866, which is known to be protonated.[23]

One of the three systems has the conventional protonation states (charged Glu559 and Asp767, and neutral His752), designated from now on as **"Standard system"**. A second one has a neutral Glu559, designated from now on as **"Glu559H system"**. The third system has His752 charged, designated from now on as **"His752H system"**. This last protonation state did not derive from the proposals put forward in the literature, but emanated from the results obtained during the development of this work.

2) Molecular dynamics (MD) simulation of the "Standard system", "Glu559H system" and "His752H system":

The three systems were subjected to ≈30 ns of MD simulation (all methodological details and analysis of these simulations can be found in Supporting Information). The MD simulations allowed the modeled active site to equilibrate but also enable us to perceive the differences between each system MD simulation and the original crystal structure.

For the MD simulations, we parameterized the substrate using the General AMBER Force Field[24] atom types and the correspondent force field parameters and the antechamber module of AMBER.[25] For cofactor we used previously determined parameters.[26] Atomic charges were obtained using ONIOM(HF/6-31G(d):amber) electrostatic potential and the Restrained Electrostatic Potential (RESP) fitting method.[27] The electrostatic potential was calculated using the substrate and cofactor within the enzyme and in the bound conformation. We did several tests prior to the decision about which method to use to calculate the electrostatic potential. The differences between the use of HF/6-31G(d), ONIOM(HF/6-31G(d):MM), ONIOM(B3LYP/6-31G(d):MM) or the charges provided by the Amber Parameter Database (http://sites.pharmacy.manchester.ac.uk/bryce/amber)[26] were very small, with a root-mean square deviation (RMSD) between 0.13 and 0.16 a.u. whichever pair of methods is compared.

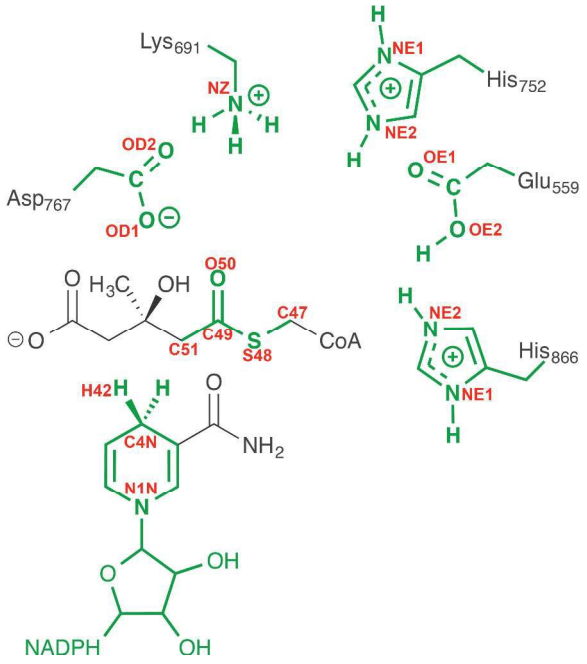

Figure 1 - Representation of the active site. High layer atoms are colored in green and atom names used throughout the article are labeled in red. There are 12094 atoms in the MM layer, not represented here for simplicity.

3) QM/MM calculations on the "Standard system", "Glu559H system" and "His752H system"

Several methodologies are currently employed in the computational study of enzymatic reaction mechanisms with QM and QM/MM theoretical levels. The cluster model approach studies the enzyme mechanism in a carefully chosen model of the enzyme active site, treated as accurately as possible.[28–32] Alternatively, full enzyme QM/MM models,[33–38] or full enzyme models with consideration of the enzyme dynamics,[39–43] are often employed. QM/MM MD approaches[42] have a steep impact on the computational cost. To mitigate the problem, several methods can be considered, such as treating the solvent implicitly,[43] use of an EVB Hamiltonian,[44] substitute the demanding QM Hamiltonian by approximate molecular orbital methods,[45–48] or separate the dynamical sampling from the QM/MM scheme.[38,49]

We opted for the last scheme, using two layered QM/MM ONIOM models, with electrostatic embedding coupling, to better replicate the electrostatic environment and the steric constraints present in the enzyme.

During the geometry optimizations, the QM high level layer consisted of 80-81 atoms and was described at the B3LYP/6-31G(d) level, while the MM low level layer (over 12,000 atoms) was described with parm99SB parameters, hard-wired in the input file. The high level layer included atoms from residues NADPH, HMG-CoA, Glu559, His866, Lys691, Asp767 and His752, as depicted in Figure 1. The truncated valences were completed by the addition of hydrogen link atoms.

Structures from the PESs were fully optimized to minima/transition state (TS). QM/MM TS structures were optimized and characterized using a Hessian matrix with all the coordinates of the QM layer. The MM layer consisted of 146 unconstrained amino acids (more than 14 Å from C49 atom - Figure 1), optimized using micro iterations, and 654 constrained amino acids. A list of the unconstrained residues ("free region") can be found in Sup-

porting Information. All water molecules were removed except the ones in the "free region" closer to the QM layer (up to 5 water molecules).

Special care was taken to assure that reactants and products remain in the same local valley as the TS's, and reactants and products were optimized from the TS after small displacements in the reaction coordinate.

"The energies shown without parenthesis correspond to free energies calculated using a larger basis set (6-311++G(2d,2p)) in the B3LYP layer, in a single-point calculation, with entropy (at 298.15 K) calculated within the ideal gas/rigid rotor/harmonic oscillator formalism, and contributions from dispersion according to the formalism of the empirical D3 long-range dispersion correction.[50] The energies shown inside parenthesis correspond to ONIOM B3LYP(6-311++G(2d,2p))-D3//AMBER potential energy. All these calculations were made with the software Gaussian 09.[51]

We explored reaction pathways in the conformation present in the crystallographic structure, but also from conformations selected from the MD trajectory (details about clustering and selection of representative structures are provided in Supporting Information). The crystallographic structure was co-crystalized with an analogue of the product. Large scale motions might be involved in the transition from the reactant state to the product state, in particular due to the exchange of the large cofactor after the first hydride transfer. Due to the modeling involved in the preparation of our systems we judged important to explore the reaction mechanism starting from conformations equilibrated to the reactant state during the MD. Therefore, for each system we selected one representative structure that gathered optimal active site configurations to catalyze the reaction, as detailed in Supporting Information.

4) Conformational sampling for system with the most favorable PES– the "Glu559H system"

It is generally accepted that an active site that provides an optimal structural framework to achieve and stabilize the transition state is among the most important catalytic features of an enzyme.[28] Reactions take place at the fs timescale, while turnover is at the ms-s timescale, which means that the enzyme has plenty of time to navigate the PES and eventually pass through these productive configurations. Hence for the protonation state with more promising activation energies, we performed a more thorough exploration of structures present in the MD conformation. The reaction pathways were studied in additional 15 representative structures of the clustered MD. Clustering the MD aimed to provide a diverse and representative sampling within a reasonable number of conformations, which is seldom possible with QM/MM MD. In this way we avoided the use of semiempirical Hamiltonians required to extensively sample the conformational space with QM/MM MD, since we believe the errors coming from low level semiempirical methods might be greater than the inaccuracies due to our reduced (albeit carefully chosen) sampling of the conformational space (clustering details are provided in Supporting Information). The representativeness of our sampling depends on several factors, namely how perfectly the representative structure of a given cluster represents the cluster average and how meaningful are the features chosen for clustering for the reaction mechanism. However, to evaluate the extent to which the sampling is complete we would have to study many more configurations, which is unfeasible at present.

Conformational entropy is not accounted for in our method (all other relevant sources are considered). The impact of neglecting this effect might not be larger than the other errors of the method/protocol, as the method used here (as well as the cluster models, that make the same approximation) generally provide free energy barriers in agreement with experimental values.[52] Again, the error in the barrier introduced by the use of semiempirical methods in this system (to recover the conformational entropy) may be quite larger than the neglect of the conformational component of the entropy.

Results and Discussion:

Standard system:

The three different protonation states did not generate highly different trajectories (Molecular dynamics analysis in SI). "Standard system" presented the lowest RMSD for the atoms in the 146 amino acid residues that surround the chemically active region (Scheme S2) of the three systems along the MD simulation. Interestingly the distance between the closest oxygens of Glu559 and Asp767 is on average 3.98±0.35 Å and after QM/MM geometry optimization rested at 3.67 Å, which is not very different from the distance found in human crystallographic structures (3.6-3.7 Å). This short distance was believed to raise the pKa of glutamic side chain and supported a neutral Glu559 in a previous reaction mechanism hypothesis.[6] We show that in the electrostatic context of the HMG-CoA-R active site, namely the triad formed by Glu559, Asp767 and Lys691, the interactions between His866 and Glu559 and between the 2'-hydroxyl group from the ribose moiety of NADPH and Asp767, allowed the two charged carboxyl side-chains to co-exist in proximity. "Standard system" trajectory also presented the shortest distance between the NADPH hydride and the substrate, with an average distance of 3.55±0.23 Å.

After QM/MM geometry optimization the active site retained crystallographic resemblances (Figure 2, Scheme S2). Nonetheless, a reaction mechanism with convincingly low activation free energy was not found. We tried the direct formation of the mevaldehyde intermediate and CoA-S^-, without passing through mevaldyl-CoA (data not shown). This pathway should require the stabilization of the negative charge at S48 in $TS1^{Standard}$ by the proton from His866. Our model orientated His866 proton towards the forming CoA-S^-, but in the resulting intermediates (CoA-S^- and mevaldehyde), His866 proton was not transferred and remained at 2.00 Å from S48. This arrangement did not provide sufficient stabilization to the transition state and resulting intermediates, probably due to the repulsion between the charged His866 and $NADP^+$($\Delta E^{\ddagger}$=(44.9)kcal·mol^{-1}, ΔE_r=(41.7)kcal·mol^{-1}, data not shown).

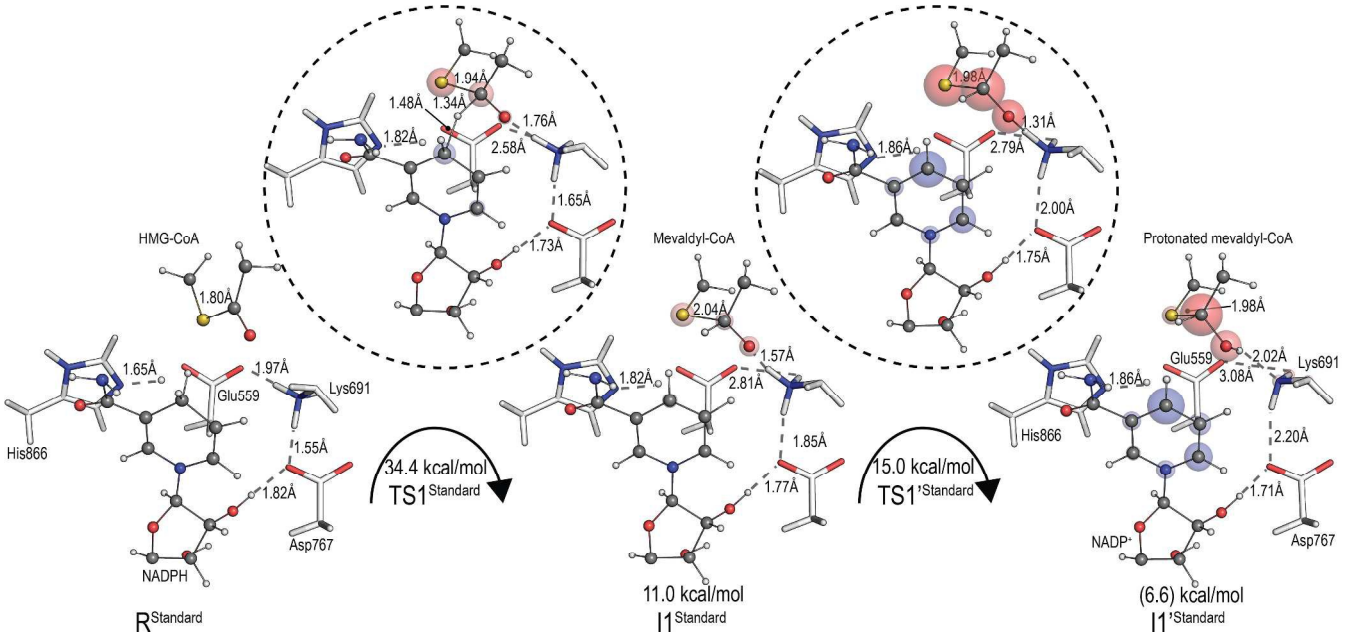

Figure 2 – First hydride transfer reaction in "Standard system". The size and color of the spheres denotes the CM5 charge variation compared to the $R^{Standard}$ structure. Blue spheres indicate positive charge variations and red spheres indicate negative charge variations.

The lowest barrier for hydride transfer was defined along the distance between the hydride and carbon C49 from HMG-CoA, with an activation free energy of 34.4(34.8) kcal·mol^{-1} and a reaction free energy of 11.0(15.1) kcal·mol^{-1} (Figure 2, Figure 3).

In the transition state ($TS1^{Standard}$, Figure 2) the hydride was at 1.34 Å from C49. The carbonyl bond distance (O50 to C49) stretched from 1.23 Å to 1.27 Å, which reflected the increased single bond character. Lys691 helped the stabilization of the negative charge developing there, but the proton was not transferred, keeping a distance of 1.76 Å. CM5 atomic charges[53] showed that the charge transferred from NADPH to the mevaldyl-CoA intermediate at $TS1^{Standard}$ was located mainly in S48, but also spread over C49 and O50. Asp767 made a hydrogen bond with Lys691 (1.65 Å) and with the hydroxyl group from the NADPH ribose (1.73 Å). Glu559 was hydrogen bonded to His866 (1.82 Å) thus weakening its interaction with Lys691 (2.58 Å).

When the hydride was fully bound to C49 (1.12 Å, $I1^{Standard}$), Lys691 remained close to the thioester oxygen of mevaldyl-CoA (1.57 Å) but never donated its proton. Despite the fact that both Glu559 and Asp767 hydrogen bonded to neighbors other than Lys691, and that Lys691 always remained very close to the negatively charged mevaldyl-CoA oxygen, it seemed that this conserved lysine was not able to provide sufficient stabilization both for the transition state and the resulting product. In fact, CM5 atomic charges showed that, in $I1^{Standard}$, the hydride negative charge was dispersed homogeneously between O50, C49 and S48.

The next step should be either the protonation of the mevaldyl-CoA intermediate or the formation of the mevaldehyde intermediate (Figure 3

2, Figure 3). We tried both pathways but protonation of the hemithioacetal by Lys691 (TS1'^{Standard}, Figure 2) led to a much more stable intermediate (I1'^{Standard}) (ΔE_r=2.3(6.6) kcal·mol^{-1}) and the activation energy required was smaller ($\Delta G^{\ddagger}$=4.0(2.1) kcal·mol^{-1}) (Figure 3). The protonated mevaldyl-CoA (I1'^{Standard}) interestingly shifted the charge predominantly to C49 and increased the positive character of $NADP^+$. The possibility of a concerted reaction pathway of the hydride and proton transfer with a more favorable activation free energy was explored but never found in subsequent calculations. We concluded that the two events were highly asynchronous.

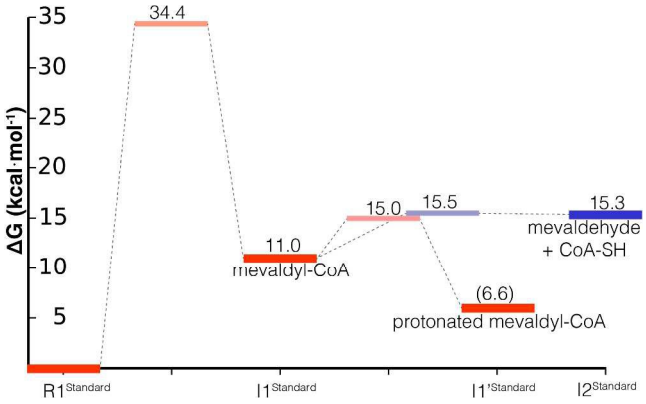

Figure 3 - Free energy profile for the first hydride transfer in the "Standard system". The different colors highlight that there are two possible pathways to form two different intermediates, either mevaldyl-CoA protonated by Lys691 (red) or mevaldehyde+CoA-SH with protonation of CoA by His866 (blue).

His752H system:

Several active site residues of HMG-CoA-R are ionizable, such as His866, Glu559, Asp767 and Lys691, and several reaction mechanism proposals assign different protonation states and acid/base roles for these residues (for a review see Haines et al.[10]). However, a role for His752 was never proposed, mainly because the *P. mevalonii* structure is more commonly used and lacks this histidine.[14,16]

We noticed that during the hydride transfer HMG-CoA O50 came closer to His752, placing the thioester oxygen between His752 and Lys691. This suggested that Lys691 and His752 might form an oxyanion hole that stabilizes the negative charge developed in the thioester oxygen.

We decided to model a charged His752 in the "His752H system". The intrinsic pKa of histidine (6.2) made this hypothesis very likely. During most of the MD simulation, the charged histidine prefers to interact with the charged Glu559, but a hydrogen bond between the thioester oxygen and His752 appeared in 8% of the trajectory time. However, after QM/MM geometry optimization of one of these structures (data not shown), Asn755 and Leu562 were pulled outwards and allowed His752 to hydrogen bond Glu559 instead of the thioester oxygen. The resulting active site was the most different from the crystallographic one with an (even though small) RMSD of the "free region" ("free region" specified in Supporting Information) of 1.48 Å (note that during the MD simulations the entire system was free to move). The hydride distance to CoA was short (2.94 Å) but the hydride trans-

fer was prohibitively high. All attempts to find a concerted hydride transfer with simultaneous protonation by His752 have failed, so we assume that there is no saddle point for the concerted mechanism.

We tried the reaction from the X-ray conformation, where Asn755 and Leu562 remained between His752 and Glu559 and allowed His752 to maintain a hydrogen bond with HMG-CoA thioester oxygen (RMSD for "free region" atoms = 0.47 Å. "Free region" specified in Supporting Information). This conformation has the lowest activation free energy for this system (Figure 4). The hypothesis was that the interaction between His752 and the substrate carbonyl, present in the crystallographic structure, polarized the bond between C49 and O50, increasing the electrophilic character of HMG-CoA that would facilitate the hydride transfer.

We found a slight polarization of the carbonyl bond in this system (the carbonyl bond length increased by 0.02 Å to 1.24 Å) and the activation free energy reached a maximum of 40.6(41.3) kcal·mol^{-1} when the hydride was located at 1.48 Å from C49 and at 1.34 Å from C4N (Figure 4). This is a very early transition state as the positive charge being created in the cofactor is repelled by the charged His752. The thioester oxygen maintained the hydrogen bond with His752 (1.78 Å) but protonation only occurred after the hydride was transferred. Lys691 was also close to the carbonyl oxygen (2.97 Å), but its main role should be to help stabilizing the Glu559 charge in combination with His866 (1.66 Å and 1.76 Å) (Figure 4 – TS1^{His752H}). At the TS1^{His752H} the charge gained by HMG-CoA was mostly localized at S48 and, to a lesser extent, at the carbonyl group of HMG-CoA (Figure 4).

When the hydride was fully transferred to C49 (1.09 Å), the His752 proton got transferred to mevaldyl-CoA and the reaction free energy dropped to –8.4(-6.2) kcal·mol^{-1}(Figure 4). With protonation (I1-Xray^{His752H}), the negative charge became localized over S48, C49 and O50 but also over His752 (Figure 4). Along this step, Lys691 and His866 hydrogen bonded Glu559, respectively 1.59 Å and 1.63 Å, and helped shield its negative charge.

The very stable protonated mevaldyl-CoA could allow for a long-lived intermediate that would permit the cofactor exchange before the formation of mevaldehyde, consistent with experimental data.[54,55] However, the lowest reaction free energy required to reach the transition state, found using the X-ray conformation, is prohibitive, even when trying a concerted proton transfer and hydride transfer transition state. Additionally, a further energy penalty might be added to the reaction free energy of His752H-Xray conformation due to the preferred His752 and Glu559 interaction found in MD trajectory.

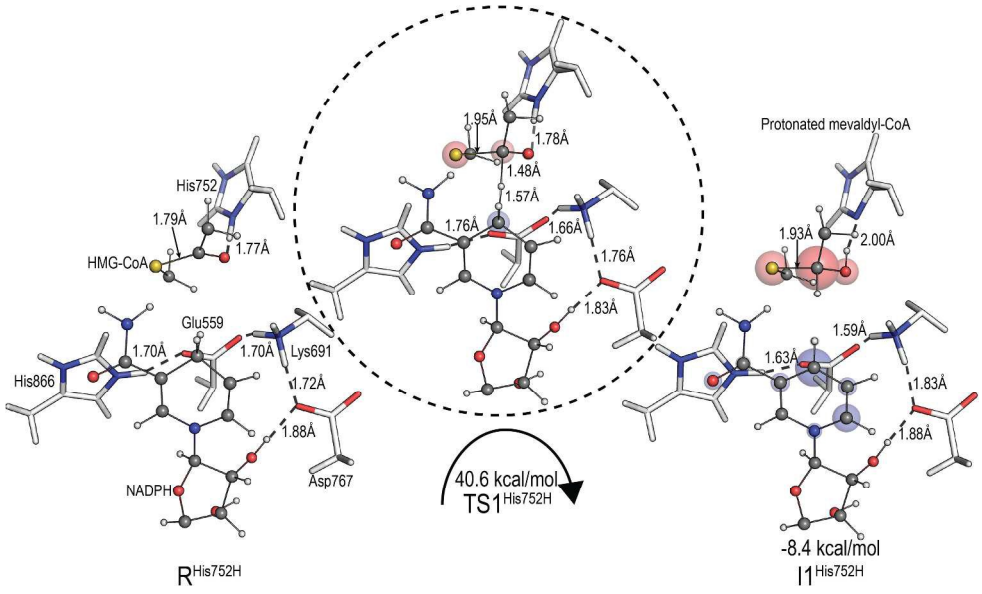

Figure 4 - High-layer structures for the hydride transfer in the His752H-Xray conformation. The size and color of the spheres denotes the CM5 charge variation compared to the R-Xray^{His752H} structure. Blue spheres indicate positive charge variations and red spheres indicate negative charge variations.

Glu559H system:

The active site organization from the "Glu559H system" conformation with most favorable reaction energies (Glu559H) has a small RMSD for the unconstrained atoms of 1.36 Å (unconstrained amino acids are specified in Supporting Information), when compared to the crystallographic structure. Notwithstanding, during the MD simulation the neutral Glu559 distanced itself from the charged His866 due to a hydrogen bond of the former with Asp767. His866 lost Glu559 as an anchor point and got placed at 5.55 Å from the HMG-CoA S48 atom. The role of His866 was proposed to be that of protonating the CoA sulfur atom when mevaldehyde was formed.[11] Nevertheless, the distancing of His866 does not exclude this hypothetical role, since His866 rests in a flexible helix that is known to close over the active site.[8,56] The other consequence of the hydrogen bond between Glu559 and Asp767 during the MD was that it displaced Glu559 from the vicinity of HMG-CoA carbonyl group. Consequentially Glu599 is no longer in an appropriate position to be the general acid that stabilizes the mevaldyl-CoA intermediate, as previously suggested for *P. mevalonii* enzyme.[14]

Our findings in the "Glu559H system" and the "Standard system" were different from earlier proposals.[10] Haines et al.[14] found that a neutral Glu559* in the prokaryotic enzyme reproduced more closely the active of the crystallographic structure, while a system with a charged Glu559* maintained less resemblances.[10] In their model the charged Glu559* deviated from the crystallographic structure active site as a consequence of the electrostatic repulsion between the negatively charged Glu559* and Asp767* residues, and due to the salt bridge between Glu559* and His866* that brought His866* deeper in the active site.[10] In the human enzyme we observed that the distance between the closest oxygens from Glu559 and Asp767 is on average 2.59±0.28 Å, which is closer than the distance found in the crystal structure (3.6-3.7 Å) and more different to the crystal structure than "Standard system".

The hydride transfer in "Glu559H system" was far more favorable than in the previous two systems (Figure 3 and Figure 4). The most favorable pathway was obtained with a structure from the MD simulation. The free activation energy was 17.8(17.9) kcal·mol^{-1} and it did generate a slightly exothermic mevaldyl-CoA intermediate, surprisingly protonated by Lys691 and not by Glu559 (ΔG_r=-1.6(-0.5) kcal·mol^{-1}). The activation free energy obtained is in close agreement with *P. mevalonii* turnover rate of 1 s^{-1} to 1 min^{-1} (18.2-20.7 kcal/mol). The reaction pathway is also similar to the previous proposal by Tabernero et al.[8] for *P. mevalonii* (Scheme 2-B) but in an active site with a neutral Glu559.

Figure 5 shows the geometries of the reactant ($R^{Glu559H}$), transition state ($TS1^{Glu559H}$) and the resulting protonated hemithioacetal ($I1^{Glu559H}$). In the optimized transition state, the transferring hydride was at 1.22 Å from C49, 1.55 Å from C4N and a 2.73 Å distance between C4N:C49 (Figure 5). Lys691 (and not Glu559) stabilized the negative charge developing at the thioester oxygen and, at the $TS1^{Glu559H}$, transferred its proton to the substrate. The Glu559 hydrogen bonded to Asp767 (1.51 Å), weakening the Lys691-Asp767 interaction (2.10 Å) and, consequently, lowering the pKa of Lys691 (Figure 5). This allowed Lys691 to protonate the thioester oxyanion. The major difference between $TS1^{Glu559H}$ and the other two previous transition states is that the charge transferred to the substrate was mainly located at C49 and O50 atoms instead of S48.

The resultant protonated mevaldyl-CoA was very stable and the reaction proceeded without major conformational changes (Figure 5).

A slightly different reaction pathway was previously reported by Haines et al.[14] for the *P. mevalonii* enzyme, with similar activation and reaction free energies ($\Delta E^{\ddagger}$=(21.8) kcal·mol^{-1}, ΔE_r=(8.3) kcal·mol^{-1}). They suggested Glu559* as the proton donor for the mevaldyl-CoA intermediate in the prokaryotic enzyme.

To evaluate this possibility in the human enzyme we had to model the "Glu559H system" directly in the X-ray conformation (Glu559H-Xray). We could not use MD sourced conformations because Glu559 exchanged its

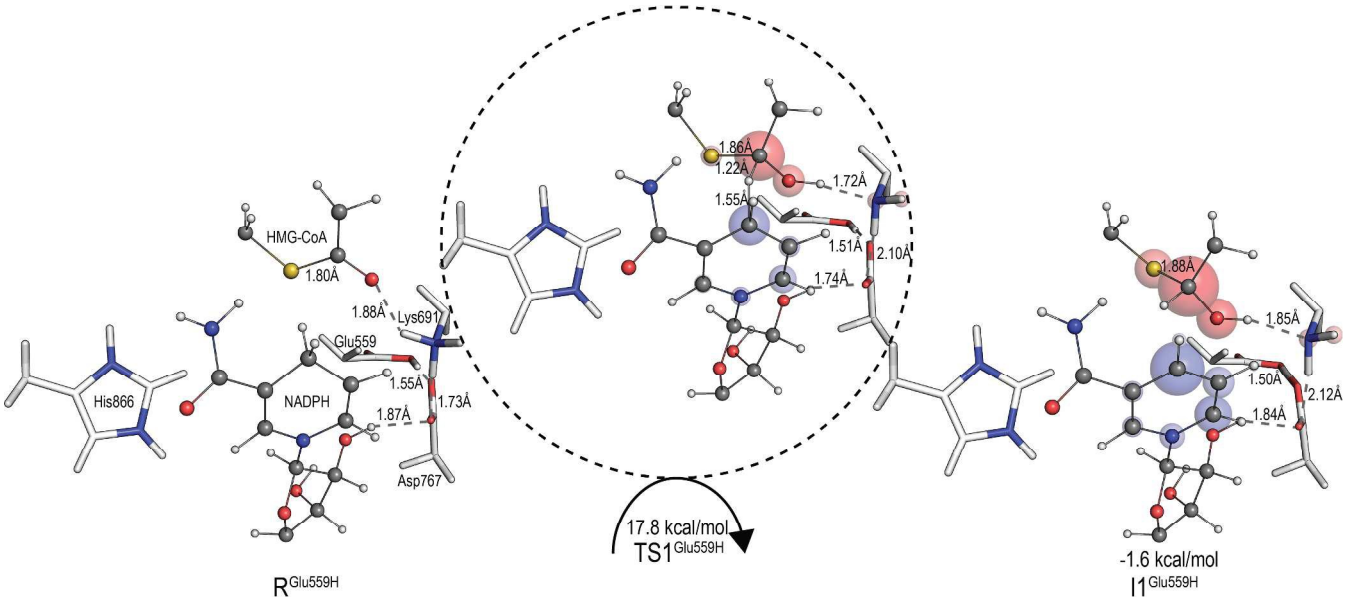

Figure 5 - Structures from the active site of the Glu559H conformation. Hydride transfer takes place simultaneously with protonation of the mevaldyl-CoA intermediate by Lys691. The size and color of the spheres denotes the CM5 charge variation compared to $R^{Glu559H}$ structure. Blue spheres indicate positive charge variations and red spheres indicate negative charge variations.

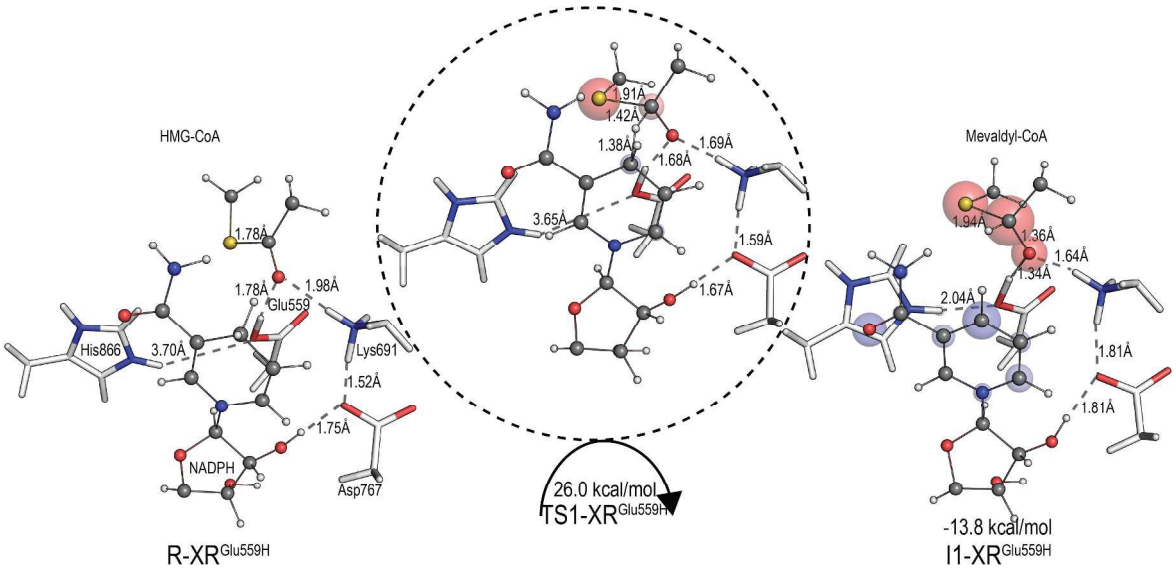

Figure 6 - Structures from the active site of Glu559H-Xray conformation. The size and color of the spheres denotes the CM5 charge variation compared to R-$Xray^{Glu559H}$ structure. Blue spheres indicate positive charge variations and red spheres indicate negative charge variations.

Table 1. Comparison of the free energy profile for the first hydride transfer in the several conformations presented for three different active site protonation states.

	ΔG (kcal·mol^{-1})				
	R	TS1	I1$^{mevaldyl\text{-}CoA}$	TS1'	I1$^{protonated\ mevaldyl\text{-}CoA}$
Standard	0	34.4(34.8)	11.0(15.1)	15.0(17.2)	2.3(6.6)
	R	TS1	I1$^{mevaldyl\text{-}CoA}$		
His752H-Xray	0	40.6(41.3)	-8.4(-6.2)		
Glu559H	0	17.8(17.9)	-1.6(-0.5)		
Glu559H-Xray	0	26.0(27.8)	-13.8(-13.9)		
	R	TS1-A	I2-A^{mevaldehyde}	TS2-A	I2'-A$^{mevaldehyde\ +\ CoA\text{-}SH}$
Glu559H-c15	0	27.2(29.6)	-1.4(0.2)	-1.4(1.8)	-5.3(0.2)

hydrogen bond from HMG-CoA carbonyl group to Asp767 early in the MD simulation and brought instead Lys691 close to HMG-CoA to provide the required stabilization.

The resulting pathway had a higher activation barrier ($\Delta G^{\ddagger}$=26.0(27.8) kcal·mol^{-1}) and in the transition state (TS1-Xray^{Glu559H}) the hydride was at a distance of 1.43 Å from C49 and 1.36 Å from C4N. The negative charge being developed in the carbonyl oxygen was stabilized by the neutral Glu559 (1.68 Å) and by Lys691 (1.69 Å) but without proton transfer to the alkoxide (Figure 6). The negative charge of Asp767 (3.84 Å away from Glu559), might hinder protonation of O50 by Glu559. Besides the Glu559 orientation, the major differences to TS1^{Glu559H} were the hydrogen bond between Lys691 and Asp767 (absent in TS1^{Glu559H}), which might increase Lys691 pKa, and the charge gained by the substrate that is mainly located at S48 (Figure 6) instead of C49.

When the mevaldyl-CoA intermediate (I1-Xray^{Glu559H}) was reached, the charge gained by mevaldyl-CoA was then homogeneously distributed throughout the S48, C49 and O50 atoms (Figure 6). Glu559 strengthened the stabilization of the thioester oxyanion (1.34 Å) but the mevaldyl-CoA intermediate was not protonated. Nevertheless, the interactions provided by Lys691, Glu559 and His866 greatly stabilized I1-Xray^{Glu559H} (ΔG_r=-13.8(-13.9) kcal·mol^{-1}) (Table 1)

With such stable intermediate we hypothesized that it was the ideal time to exchange the cofactor. This would agree with the experimental results that suggest the cofactor exchange prior to mevaldehyde formation.[55,57] Nevertheless, such stable mevaldyl-CoA intermediate would make the reaction very much exothermic, and not almost athermic, as experimentally deduced from the reversibility of the reaction.[12]

The activation free energy to obtain mevaldyl-CoA stabilized by Glu559 is 8.2(9.9) kcal·mol^{-1} higher than the required when Lys691 fulfills this role (Table 1). We were also unable to replicate this pathway with credible activation energies starting from different MD sourced conformations (results not shown).

The conformation present in the crystallographic structure was obtained with a mevalonate analogue inside the active site, instead of HMG-CoA, and a resolution of 2.0 Å and thus it requires prudence. On the other hand, the most important conformational change from the MD simulation, the formation of the hydrogen bond between Glu559 and Asp767, was expected due to the close distance found in the crystallographic structure between Glu559 and Asp767 (3.55 Å). This strengthened our confidence in the conformations generated by the MD simulation.

Conformational sampling in Glu559H system.

It is important to remark that we did not take into account the free energy differences between the three protonation states. Nevertheless the activation free energy gap that differentiates both pathways (Glu559 or Lys691 as general acids) in "Glu559H system" from the pathways found in the "Standard System" and "His752H system" makes it safe to assume that the energy differences between the different protonation states will not overcome the differences found in the reaction mechanisms.

Therefore, we consider "Glu559H system" the only system that presents physiologic competent activation and reaction free energies and decided to explore the reaction mechanism in representative structures of the clustered MD simulation (Figure S1 and Table S2).

Starting from fifteen representative conformations (that represent 61% of the simulation time), we noted that ten (one for each of ten clusters that, altogether, represent 38% of the simulation time) generated mevaldyl-CoA intermediate protonated at the carbonyl oxygen O50 by Lys691, in the same way as the Glu559H mechanism presented above. Two conformations generated mevaldyl-CoA intermediate but not protonated at the carbonyl oxygen and the remaining three conformations the mevaldehyde intermediate and CoA- S^- were directly obtained.

Mevaldyl-CoA intermediate protonated by Lys691 (conformations c1 to c10)

The lower-energy intermediates and lower activation free energies are found in this group. Nevertheless, the activation free energies (19.1(20.9) to (37.8 kcal·mol^{-1}) and the reaction energies ((-13.6) to (15.2) kcal·mol^{-1}) fluctuate considerably.

For the two most favorable conformations (beyond the Hamiltonian energies we also calculated the free energy barriers)(Table S2), Glu559H-c1 ($\Delta G^{\ddagger}$=19.1(20.9) kcal·mol^{-1}, ΔG_r=-3.7(-2.4) kcal·mol^{-1}) and Glu559H-c2 ($\Delta G^{\ddagger}$=20.3(21.8) kcal·mol^{-1}, ΔG_r=-4.4(-1.3) kcal·mol^{-1}), that represent respectively 11% and 1% (Figure S1 and Table S2) of the simulation time, shared a very similar active site organization and bore significant resemblances to Glu559H.

Moreover, the reverse reactions in these two conformations were possible, as the experimental results imply and contrasting to the pathway found in the crystal structure.[13]

Deprotonated mevaldyl-CoA (conformations c11 and c12)

Two conformations, representative of 5% of the simulation time, generated the mevaldyl-CoA intermediate without protonation of the carbonyl oxygen. However, the resulting intermediates were very high-energy intermediates (as such we have only calculated the electronic energy barriers) ($\Delta E^{\ddagger}$=(31.4) kcal·mol^{-1}, (ΔE_r=(17.2) kcal·mol^{-1} and $\Delta E^{\ddagger}$=(29.5) kcal·mol^{-1}, ΔE_r=(26.8) kcal·mol^{-1}).

One of the conformations lacked the hydrogen bond between the 2' hydroxyl group from the ribose nucleotide of NADPH and the carboxyl group from Asp767. Consequentially, interaction between Asp767 and Lys691 was strengthened and hindered the protonation of the mevaldyl-CoA intermediate by Lys691. The other conformation showed a longer distance between Lys691 and the substrate hemithioacetal oxygen (2.78 Å) that hindered the protonation by Lys691.

Mevaldehyde and CoA-S- (conformations c13 to c15)

Two of the three conformations (c13 and c14, representing respectively 18% and 1% of the simulation time) did not have a hydrogen bond between the ribose and Asp767, which strengthened the Asp767:Lys691 interaction and deviated Lys691 away from the HMG-CoA carbonyl oxygen. This impacted profoundly on the stabilization of the TS1 and, as a result, the activation barriers to reach the first hydride transfer became prohibitive ($\Delta E^{\ddagger}$=(37.2) kcal·mol^{-1}, ΔE_r=(12.5) kcal·mol^{-1} and $\Delta E^{\ddagger}$=(46.8) kcal·mol^{-1}, ΔE_r=(-1.9) kcal·mol^{-1}).

The remaining conformation (c15) is the most favorable within this pathway, with an activation free energy of 27.2(29.6) kcal·mol^{-1}, but represents less that 1% of the simulation time. Glu559H-c15 conformation had a sub-

optimal orientation of Lys691 to stabilize the transition state but instead had a close interaction between His866 and S48 (2.57 Å) (Figure 7). The short distance between His866 and S48 found in X-ray diffraction structures along with the low activity of the His866 mutant, suggested the charged His866 to be the general acid for protonation of the CoA anion upon decomposition of the hemithioacetal intermediate.[9,13] In Glu559H-c15 conformation, this interaction allowed the charge gained with the hydride transfer to be shifted mainly to S48 and resulted in substrate breakdown with formation of CoA-S$^-$ thioanion and mevaldehyde. Subsequent protonation of CoA-S$^-$ by His866 generates a very stable intermediate -5.3(0.2) kcal·mol^{-1} but the overall activation barrier is still 9.4(11.6) kcal·mol^{-1} higher than the most favorable reaction in the mevaldyl-CoA protonated by Lys691 pathway (Figure 5 and Figure 7).

Among the remaining representative structures, the ones that represent more than 5% of the simulation time, did not possess any group surrounding hemithioacetal oxygen O50, which would render the hydride transfer very unlikely.

Assembling all the results obtained with "Glu559H system", several aspects support the formation of mevaldyl-CoA intermediate protonated by Lys691, as in the MD conformation GLU559H (Figure 5). Namely, this pathway is the most common among the representative structures of the clustered MD simulation, presented the overall lowest activation free energy, retained the reversibility of the reaction, as observed experimentally,[11] and the stability found for the resulting mevaldyl-CoA intermediate should allow a long lived intermediate to permit the cofactor exchange. The shift of the neutral Glu559 towards Asp767 observed in MD conformations lowers Lys691 pKa and places it in a suitable site to allow a stronger stabilization of the mevaldyl-CoA intermediate, not found in any other system or conformation. This Glu559 conformational change seen during the MD simulation seems appropriate due to the short distance from the negatively charged Asp767.

Considering all 11 conformations that protonate mevaldyl-CoA with Lys691, the observed (or apparent) k_{cat} according to equation 1:

$$k_{cat} = k\frac{k_B T}{h}\sum_{i=1}^{n} P_i\, e^{\frac{-\Delta G_i^{0\ddagger}}{RT}} \quad (1)$$

where P_i is the probability of finding the enzyme in the reactant state i and $\Delta G_i^{0\ddagger}$ is the corresponding barrier free energy, is 19.3 kcal·mol^{-1} considering an equal probability for each conformation. The 95% lower and upper confidence limits for the average rate constant, determined by bootstrap (1000 samples), corresponds to a free energy barrier between 18.7 and 26.4 kcal·mol^{-1}. The observed free energy barrier for *P. mevalonii* calculated from the turnover rate of 1 s^{-1} to 1 min^{-1} (18.2-20.7 kcal·mol^{-1}) compares well with the 19.3 kcal·mol^{-1} values found here, despite the still large confidence interval. It is relevant to note that most research works present uncertainties in the form of standard deviation, which correspond to about one half of the 95% confidence interval presented here. Therefore, the confidence intervals that we show constitute a very stringent test of statistical convergence.

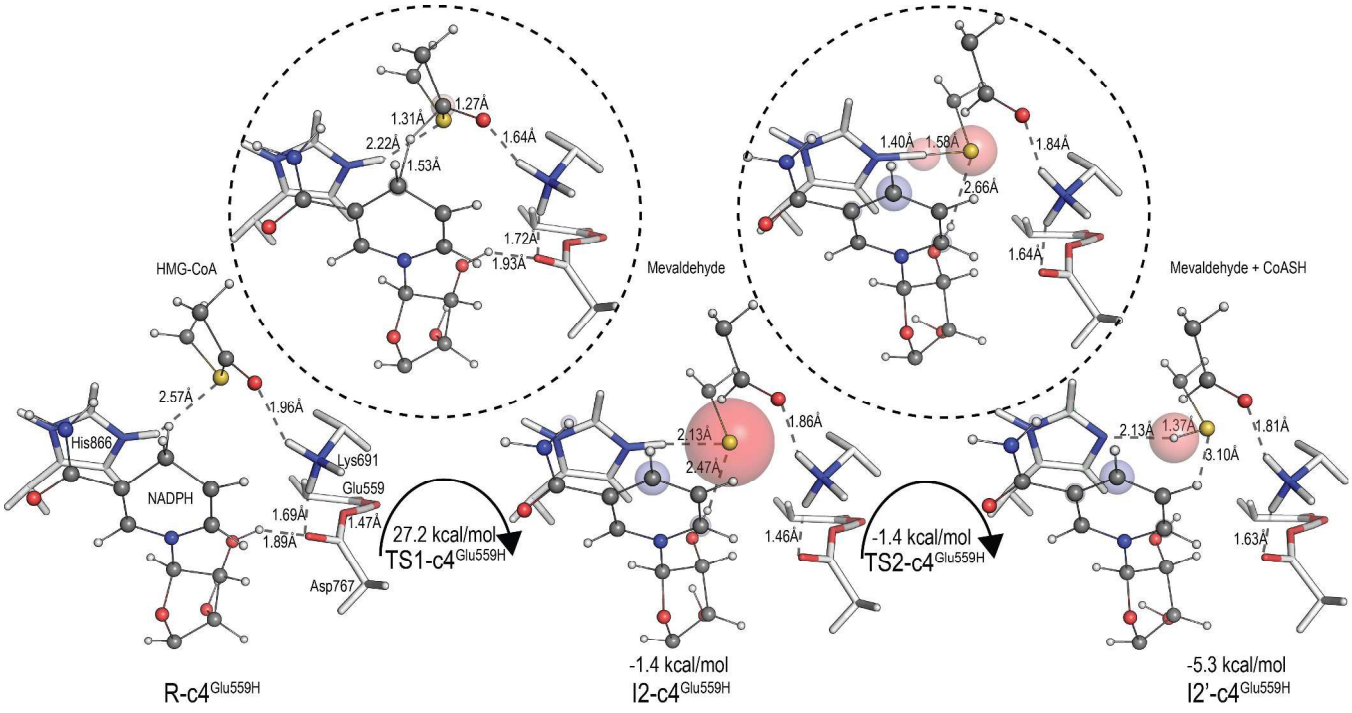

Figure 7 - First hydride transfer for the Glu559H-c15 system. The size and color of the spheres denotes the CM5 charge variation compared to R-c15^{Glu559H} structure. Blue spheres indicate positive charge variations and red spheres indicate negative charge variations.

The first hydride transfer is expected to be the rate-limiting step, due to the lower electrophilicity of the thioester compared to the aldehyde. Haines et al.[14] found the first hydride transfer to have an activation energy of 21.8 kcal·mol^{-1} while the second hydride transfer has a lower activation barrier by 2.9 kcal·mol^{-1}.

Conclusions

The work presented here aimed to elucidate the reaction mechanism of the first reduction step of HMG-CoA-R, the rate-limiting step, resorting to MD and QM/MM calculations. We considered three different active-site protonation states and thoroughly compared the reaction mechanism in the three systems.

The active site of the "His752H system" rendered the lowest resemblances to the crystallographic structure and the highest activation energies for the hydride transfer (Figure 4) making this hypothesis unlikely. The system with standard protonation states ("Standard system") retained the best resemblances to the crystallographic structure but a strong interaction between Lys691 amino group and charged Asp767 raised Lys691 pKa and denied sufficient stabilization to mevaldyl-CoA alkoxide.

We found the reaction pathway with the overall lowest activation free energy (17.8 kcal·mol^{-1}) in the system where Glu559 is neutral ("Glu559H system"). The pathway with lowest activation free energies and more frequently found in representative structures of the clustered MD simulation implies protonation of mevaldyl-CoA

with Lys691. The observed activation free energy (i.e., the single activation free energy that produces the rate constant given by eq. 1) for the 11 conformations that protonate mevaldyl-CoA with Lys691 (19.1 kcal.mol^{-1}) agrees with the overall *P. mevalonii* turnover rate of 1 s^{-1} to 1 min^{-1}.

The dispersion of activation and reaction free energies found in the conformations where mevaldyl-CoA is protonated by Lys691 is considerable. Therefore, it is not totally impossible that other mechanisms, which were seen to lead to very high barriers, become eventually competitive with the chosen one, if highly productive conformations could be found. Despite not impossible, this scenario is however very unlikely.

The most distinct characteristic in "Glu559H" MD conformations is the hydrogen bond between Glu559 and Asp767, which moved Glu559 away from the substrate HMG-CoA. Glu559 conformational change seems reasonable due to the close distance between Glu559 and Asp767 found in the crystallographic structure. This hindered Glu559 to act as a general acid during the first reduction step, as suggested by both the crystallographic structure[6] and the computational study on prokaryotic HMG-CoA-R.[14] Consequently, Lys691 became more acidic and facilitated the first hydride transfer by stabilizing the negative charge developed at the thioester oxygen, through protonation.

The most favorable reaction pathway assigns a catalytic role for Lys691 that agrees well with the impairment in catalysis found for Lys691 mutant. [12] This pathway generates a stable mevaldyl-CoA intermediate that should permit the cofactor exchange and does not hinder the reverse reaction to occur, as verified experimentally.

Catalysis of the hydride transfer with formation of the mevaldehyde, instead of the tetrahedral mevaldyl-CoA intermediate, was also explored starting from a more suitable conformation (Figure 7). His866, however, did not provide sufficient stabilization to the negative charge developed at the thioester sulphur in the transition state structure.

Exploring the MD conformations and comparing with the X-ray structure permitted to scrutinize the important roles of the neutral Glu559 and charged Asp767. Glu559 was crucial, together with the ribose moiety from NADPH, to hydrogen bond Asp767 and therefore increased Lys691 acidity, which allowed mevaldyl-CoA protonation, facilitating the hydride transfer.[8,11] The lack of this Glu559-Asp767 interaction might explain the low turnover found by Frimpong et al.[11] for the Glu559 and Asp767 mutants.

This work provides the most favorable reaction pathway for the first hydride transfer in HMG-CoA-R by comparison with alternative pathways within different HMG-CoA-R active site protonation states. The rate constants resulting from the calculated energies do not include recrossing and tunneling effects, known to provide a measurable contribution for the observed rate in hydride transfer steps involving cofactors such as NADPH, but representing only a very minor effect on the "observed, apparent free energy barrier". Nevertheless, due to the large activation energy differences between the studied pathways, the conclusions should not be altered. More accurate energy profiles will require estimation of these effects, which in the very similar reaction mechanism catalyzed by L-Lactate Dehydrogenase amount to 2-3 kcal·mol^{-1},[58,59] and systematic consideration of all active site conformations.

Acknowledgements

This work has been funded by FEDER/COMPETE and Fundação para a Ciência e a Tecnologia (FCT) through grants no. PEst-C/EQB/LA0006/2011 and EXCL/QEQ-COM/0394/2012.

Oliveira E.F. thanks FCT for a doctoral scholarship (SFRH/BD/77625/2011).

Conflict of Interests

The authors declare no competing interests.

Author Contributions

Oliveira E.F. performed all the calculations. Cerqueira N.M.F.S.A. contributed for the design of the computational experiments. Fernandes P.A. and Ramos M.J. designed the computational experiments and supervised all the work. The manuscript was written through contributions of Oliveira E.F., Fernandes P.A. and Ramos M.J.. All authors have given approval to the final version of the manuscript.

Electronic Supporting Information

Frimpong et al.[11] reaction mechanism proposal for HMG-CoA-R. pKa predictions for active site residues; methodological details of the MD simulations; list of "free region" residues in QM/MM models; representation of the active sites from the structures selected from the MD simulations and from the crystal structure; energy profiles for the conformations studied in "Glu559H system"; RMSF and RMSD analysis of the MD simulations; cartesian coordinates from TS structures.

References

(1) Edwards, P. A.; Ericsson, J. *Annu. Rev. Biochem.* **1999**, *68*, 157–185.

(2) Lange, B. M.; Rujan, T.; Martin, W.; Croteau, R. *Proc. Natl. Acad. Sci. U. S. A.* **2000**, *97*, 13172–13177.

(3) Bochar, D. A.; Stauffacher, C. V.; Rodwell, V. W. *Mol. Genet. Metab.* **1999**, *66*, 122–127.

(4) Istvan, E. S. *Curr. Opin. Struct. Biol.* **2001**, *11*, 746–751.

(5) Istvan, E. *Biochim. Biophys. Acta - Mol. Cell Biol. Lipids* **2000**, *1529*, 9–18.

(6) Istvan, E. S.; Palnitkar, M.; Buchanan, S. K.; Deisenhofer, J. *EMBO J.* **2000**, *19*, 819–830.

(7) Istvan, E. S.; Deisenhofer, J. *Science* **2001**, *292*, 1160–1164.

(8) Tabernero, L.; Bochar, D. a; Rodwell, V. W.; Stauffacher, C. V. *Proc. Natl. Acad. Sci. U. S. A.* **1999**, *96*, 7167–7171.

(9) Hedl, M.; Tabernero, L.; Stauffacher, C. V.; Rodwell, V. W. *J. Bacteriol.* **2004**, *186*, 1927–1932.

(10) Haines, B. E.; Wiest, O.; Stauffacher, C. V. *Acc. Chem. Res.* **2013**, *46*, 2416–2426.

(11) Frimpong, K.; Rodwell, V. *J. Biol. Chem.* **1994**, *269*, 11478–11483.

(12) Bochar, D.; Stauffacher, C.; Rodwell, V. *Biochemistry* **1999**, 15848–15852.

(13) Li, D.; Gui, J.; Li, Y.; Feng, L.; Han, X.; Sun, Y.; Sun, T.; Chen, Z.; Cao, Y.; Zhang, Y.; Zhou, L.; Hu, X.; Ren, Y.; Wan, J. *J. Chem. Inf. Model.* **2012**, *52*, 1833–1841.

(14) Haines, B. E.; Steussy, C. N.; Stauffacher, C. V; Wiest, O. *Biochemistry* **2012**, *51*, 7983–7995.

(15) Rétey, J.; von Stetten, E.; Coy, U.; Lynen, F. *Eur. J. Biochem.* **1970**, *15*, 72–76.

(16) Steussy, C. N.; Critchelow, C. J.; Schmidt, T.; Min, J.-K.; Wrensford, L. V; Burgner, J. W.; Rodwell, V. W.; Stauffacher, C. V. *Biochemistry* **2013**, *52*, 5195–5205.

(17) Gluza, K.; Kafarski, P. In *Drug Discovery*; El-Shemy, H., Ed.; InTech, 2013; pp 325–373.

(18) Haro, D.; Marrero, P. F.; Hegardt, F. G. *Biochem. Biophys. Res. Commun.* **1985**, *132*, 598–604.

(19) Istvan, E. *Atheroscler. Suppl.* **2003**, *4*, 3–8.

(20) Anandakrishnan, R.; Aguilar, B.; Onufriev, A. V. *Nucleic Acids Res.* **2012**, *40*, W537–W541.

(21) Li, H.; Robertson, A.; Jensen, J. *Proteins* **2005**, *61*, 704–721.

(22) Hong, M. K.; Ribeiro, A. J. M.; Kim, J. K.; Ngo, H. P. T.; Kim, J.; Lee, C. H.; Ahn, Y. J.; Fernandes, P. A.; Li, Q.; Ramos, M. J.; Kang, L. W. *Acta Crystallogr. Sect. D Biol. Crystallogr.* **2014**, *70*, 1297–1310.

(23) Darnay, B. G.; Rodwell, V. W. *J. Biol. Chem.* **1993**, *268*, 8429–8435.

(24) Cornell, W. D.; Cieplak, P.; Bayly, C. I.; Gould, I. R.; Merz, K. M.; Ferguson, D. M.; Spellmeyer, D. C.; Fox, T.; Caldwell, J. W.; Kollman, P. A. *J. Am. Chem. Soc.* **1995**, *117*, 5179–5197.

(25) Wang, J.; Wang, W.; Kollman, P. A.; Case, D. A. *J. Mol. Graph. Model.* **2006**, *25*, 247–260.

(26) Holmberg, N.; Ryde, U.; Bülow, L. *Protein Eng.* **1999**, *12*, 851–856.

(27) Bayly, C. I.; Cieplak, P.; Cornell, W.; Kollman, P. A. *J. Phys. Chem.* **1993**, *97*, 10269–10280.

(28) Siegbahn, P. E. M.; Himo, F. *Wiley Interdiscip. Rev. Comput. Mol. Sci.* **2011**, *1*, 323–336.

(29) Lind, M. E. S.; Himo, F. *ACS Catal.* **2014**, *4*, 4153–4160.

(30) Ribeiro, A. J. M.; Alberto, M. E.; Ramos, M. J.; Fernandes, P. A.; Russo, N. *Chem. - A Eur. J.* **2013**, *19*, 14081–14089.

(31) Dourado, D. F. A. R.; Fernandes, P. A.; Ramos, M. J.; Mannervik, B. *Biochemistry* **2013**, *52*, 8069–8078.

(32) Alberto, M. E.; Pinto, G.; Russo, N.; Toscano, M. *Chem. - A Eur. J.* **2015**, *21*, 3736–3745.

(33) Pang, J.; Li, X.; Morokuma, K.; Scrutton, N. S.; Sutcliffe, M. J. *J. Am. Chem. Soc.* **2012**, *134*, 2367–2377.

(34) Liao, R.-Z.; Thiel, W. *J. Phys. Chem. B* **2013**, *117*, 1326–1336.

(35) Calixto, A. R.; Brás, N. F.; Fernandes, P. a.; Ramos, M. J. *ACS Catal.* **2014**, *4*, 3869–3876.

(36) van der Kamp, M. W.; Mulholland, A. J. *Biochemistry* **2013**, *52*, 2708–2728.

(37) Dokainish, H. M.; Gauld, J. W. *ACS Catal.* **2015**, *5*, 2195–2202.

(38) da Silva Gonçalves, A.; França, T. C. C.; Caetano, M. S.; Ramalho, T. C. *J. Biomol. Struct. Dyn.* **2014**, *32*, 301–307.

(39) Jitonnom, J.; Limb, M. A. L.; Mulholland, A. J. *J. Phys. Chem. B* **2014**, *118*, 4771–4783.

(40) Brunk, E.; Kellett, W. F.; Richards, N. G. J.; Rothlisberger, U. *Biochemistry* **2014**, *53*, 3830–3838.

(41) Schopf, P.; Mills, M. J. L.; Warshel, A. *Proc. Natl. Acad. Sci. U. S. A.* **2015**, *112*, 4328–4333.

(42) Yang, Z.; Doubleday, C.; Houk, K. N. *J. Chem. Theory Comput.* **2015**, *11*, 5606–5612.

(43) Su, P. C.; Tsai, C. C.; Mehboob, S.; Hevener, K. E.; Johnson, M. E. *J. Comput. Chem.* **2015**, *36*, 1859–1873.

(44) Roca, M.; Messer, B.; Hilvert, D.; Warshel, A. *Proc. Natl. Acad. Sci.* **2008**, *105*, 13877–13882.

(45) Lodola, A.; Mor, M.; Zurek, J.; Tarzia, G.; Piomelli, D.; Harvey, J. N.; Mulholland, A. J. *Biophys. J.* **2007**, *92*, L20–L22.

(46) Lodola, A.; Sirirak, J.; Fey, N.; Rivara, S.; Mor, M.; Mulholland, A. J. *J. Chem. Theor. Comp.* **2010**, *6*, 2948–2960.

(47) Sanchez-Martinez, M.; Marcos, E.; Tauler, R.; Field, M.; Crehuet, R. *J. Phys. Chem. B* **2013**, *117*, 14261–14272.

(48) Ferrer, S.; Tuñón, I.; Martí, S.; Moliner, V.; Garcia-Viloca, M.; González-Lafont, À.; Lluch, J. M. *J. Am. Chem. Soc.* **2006**, *128*, 16851–16863.

(49) Cooper, A. M.; Kästner, J. *ChemPhysChem* **2014**, *15*, 3264–3269.

(50) Grimme, S.; Antony, J.; Ehrlich, S.; Krieg, H. *J. Chem. Phys.* **2010**, *132*, 154104.

(51) Frisch, M. J.; Trucks, G. W.; Schlegel, H. B.; Scuseria, G. E.; Robb, M. A.; Cheeseman, J. R.; Scalmani, G.; Barone, V.; Mennucci, B.; Petersson, G. A.; Nakatsuji, H.; Caricato, M.; Li, X.; Hratchian, H. P.; Izmaylov, A. F.; Bloino, J.; Zheng, G.; Sonnenberg, J. L.; Hada, M.; Ehara, M.; Toyota, K.; Fukuda, R.; Hasegawa, J.; Ishida, M.; Nakajima, T.; Honda, Y.; Kitao, O.; Nakai, H.; Vreven, T.; Montgomery Jr., J. A.; Peralta, J. E.; Ogliaro, F.; Bearpark, M.; Heyd, J. J.; Brothers, E.; Kudin, K. N.; Staroverov, V. N.;

Kobayashi, R.; Normand, J.; Raghavachari, K.; Rendell, A.; Burant, J. C.; Iyengar, S. S.; Tomasi, J.; Cossi, M.; Rega, N.; Millam, J. M.; Klene, M.; Knox, J. E.; Cross, J. B.; Bakken, V.; Adamo, C.; Jaramillo, J.; Gomperts, R.; Stratmann, R. E.; Yazyev, O.; Austin, A. J.; Cammi, R.; Pomelli, C.; Ochterski, J. W.; Martin, R. L.; Morokuma, K.; Zakrzewski, V. G.; Voth, G. A.; Salvador, P.; Dannenberg, J. J.; Dapprich, S.; Daniels, A. D.; Farkas, Ö.; Foresman, J. B.; Ortiz, J. V.; Cioslowski, J.; Fox, D. J. Gaussian 09, Revision D.01. *Gaussian, Inc.*, 2009.

(52) Ribeiro, A. J. M.; Santos-Martins, D.; Russo, N.; Ramos, M. J.; Fernandes, P. A. *ACS Catal.* **2015**, *5*, 5617–5626.

(53) Marenich, A. V.; Jerome, S. V.; Cramer, C. J.; Truhlar, D. G. *J. Chem. Theory Comput.* **2012**, *8*, 527–541.

(54) Bensch, W. R.; Rodwell, V. W. *J. Biol. Chem.* **1970**, *245*, 3755–3762.

(55) Qureshi, N.; Dugan, R. E.; Cleland, W. W.; Porter, J. W. *Biochemistry* **1976**, *15*, 4191–4197.

(56) Lawrence, C. M.; Rodwell, V. W.; Stauffacher, C. V. *Science* **1995**, *268*, 1758–1762.

(57) Jordan-Starck, T. C.; Rodwell, V. W. *J. Biol. Chem.* **1989**, *264*, 17913–17918.

(58) Świderek, K.; Tuñón, I.; Martí, S.; Moliner, V. *ACS Catal.* **2015**, *5*, 1172–1185.

(59) Kamerlin, S. C. L.; Warshel, A. *J. Phys. Org. Chem.* **2010**, *23*, 677–684.